ZONAL STRUCTURE AND MERIDIONAL DRIFT OF LARGE-SCALE SOLAR MAGNETIC FIELDS

E. V. IVANOV and V. N. OBRIDKO

IZMIRAN, 142190, Troitsk, Moscow Region, Moscow, Russia

Abstract. Digitized synoptic charts of photospheric magnetic fields were analyzed for the past 4 incomplete solar activity cycles (1969–2000). The zonal structure and cyclic evolution of large-scale solar magnetic fields were investigated using the calculated values of the radial B_r, $|B_r|$, meridional B_θ, $|B_\theta|$, and azimuthal B_φ, $|B_\varphi|$ components of the solar magnetic field averaged over a Carrington rotation (CR). The time–latitude diagrams of all 6 parameters and their correlation analysis clearly reveal a zonal structure and two types of the meridional poleward drift of magnetic fields with the characteristic times of travel from the equator to the poles equal to ∼16–18 and ∼2–3 years. A conclusion is made that we observe two different processes of reorganization of magnetic fields in the Sun that are related to generation of magnetic fields and their subsequent redistribution in the process of emergence from the field generation region to the solar surface. Redistribution is supposed to be caused by some external forces (presumably, by sub-surface plasma flows in the convection zone).

1. Introduction

Large-scale solar magnetic fields play an important role in the global organization of solar activity and formation of the heliosphere. Their structure, evolution, and rotation have been thoroughly studied during the past 30 years (e.g., see Wilcox and Howard, 1970; McIntosh, 1972, 1992; Stenflo, 1974, 1989, 1992; Duvall, 1979; Howard and LaBonte, 1980; LaBonte and Howard, 1982; Snodgrass, 1983, 1984; Snodgrass and Ulrich, 1990; Hoeksema and Scherrer, 1987; Makarov and Sivaraman, 1989; Antonucci, Hoeksema, and Scherrer, 1990; Howard and Harvey, 1990; Ambrož, 1992; Komm, Howard, and Harvey, 1993a, b; Wilson, 1994; Ivanov, 1986, 1994, 1995; Makarov and Makarova, 1996; Makarov and Tlatov, 1997; Ulrich *et al.*, 1988; Ulrich, 1998; Benevolenskaya, 1996, 1998a, b; Benevolenskaya *et al.*, 1999; Erofeev, 1997, 1999; Obridko and Shelting, 1997–2000; Ananyev and Obridko, 1999; Callebaut *et al.*, 1999; and many others). Significant progress in the study of sub-surface magnetic fields in the convection zone by helioseismological methods was made in the recent five years (see, in particular, Giles *et al.*, 1997; Giles, Duvall, and Scherrer, 1998; Giles and Duvall, 1998; Schou, 1999; Giles, 1999; Howe, Komm, and Hill, 1999; Howe *et al.*, 2000; Antia and Basu, 2000). In our previous paper (Ivanov, Obridko, and Ananyev, 2001), we analyzed the sector structure and rotation of large-scale solar magnetic fields (LSSMF) using the longitudinal component of the photospheric magnetic field from digitized daily

synoptic charts. In this paper, we study the LSSMF zonal structure and meridional drift using the calculated values of the radial B_r, $|B_r|$, meridional B_θ, $|B_\theta|$, and azimuthal B_φ, $|B_\varphi|$ components of the solar magnetic field averaged over one Carrington rotation (CR). We apply the methods of time–latitude diagrams and correlation analysis to the synoptic charts of photospheric magnetic fields for the period of 1969–2000 (cycles 20–23). In Section 2 we discuss the experimental data and methods of analysis. Section 3 deals with the zonal structure, meridional drift, and cyclic evolution of LSSMF. The main results are discussed in Section 4.

2. Experimental Data and Methods of Analysis

Analysis of the zonal structure, meridional drift, and cyclic evolution of large-scale solar magnetic fields is based on Stanford (WSO) observations of the longitudinal component of the photospheric magnetic field since 1976. To extend the time interval under consideration back to cycle 20, we supplemented these observations with the data from two other observatories: Mt. Wilson and Kitt Peak. The Stanford data cover an interval of about 25 years (1976–2000). The interval from January 1969 through November 1978 (CR 1486–1648) is covered by Mt.Wilson photospheric synoptic maps obtained by the R. Howard team and the period from December 1974 through July 1984 (CR 1622–1751) by the maps from the Kitt Peak Observatory obtained by the research team under J. Harvey. All observations were reduced to a single scale by comparing the overlapping data from different observatories. This gave us a continuous series of observations for 1969–2000. In the synoptic maps, we selected 15 heliolatitudes evenly spaced by $10°$ over the latitude region of $\pm 70°$. The Carrington longitudes were digitized at $5°$ steps on the Stanford maps and at $10°$ steps on the Mt.Wilson maps. Thus, we obtained for each CR a two-dimensional data base (72×15 points for Stanford and 36×15 points for Mt. Wilson) comprising magnetic field measurements on the solar surface. The used sequence of the synoptic maps provides a time series of data from January 1969 to December 2000 digitized in heliolatitude and heliolongitude. It should be noted that the most reliable and uniform data series begins since 1976. The Mt. Wilson data from August 1965 through December 1978 digitized by Stenflo have a resolution in longitude about twice as low as the Stanford data, although it has more to do with the problem of digitizing hand drawn synoptic charts than with actual resolution of observations. The zonal structure and evolution of LSSMF were analyzed using daily magnetic field values from the synoptic maps for 1969–2000 (CR 1543–1971). The observational data were analyzed in a special way to calculate the daily radial B_r, meridional B_θ, and azimuthal B_φ components of the solar magnetic field at 15 heliolatitudes evenly spaced by $10°$ over the latitude region of $\pm 70°$. Calculations were performed for the photospheric level ($r = 1R_0$) under a potential approximation.

The solar magnetic field under a potential approximation can be represented as a function of latitude θ, longitude φ, and the distance to the center of the Sun r using the method of expansion into spherical harmonics:

$$B_r = \sum P_n^m(\cos\vartheta)(g_{nm}\cos m\varphi + h_{nm}\sin m\varphi) \times$$
$$\times ((n+1)(R_0/R)^{n+1} - n(R/R_s)^{n-1}c_n), \tag{1}$$

$$B_\vartheta = -\sum \frac{\partial P_n^m(\cos\vartheta)}{\partial\vartheta}(g_{nm}\cos m\varphi + h_{nm}\sin m\varphi) \times$$
$$\times ((R_0/R)^{n+2} + (R/R_s)^{n-1}c_n), \tag{2}$$

$$B_\varphi = -\sum \frac{m}{\sin\vartheta} P_n^m(\cos\vartheta)(h_{nm}\cos m\varphi - g_{nm}\sin m\varphi) \times$$
$$\times ((R_0/R)^{n+2} + (R/R_s)^{n-1}c_n), \tag{3}$$

where $0 \leq m \leq n < N$ (we assume $N = 9$); $c_n = -(R_0/R_s)^{n+2}$, P_n^m are the Legendre polynomials, and g_{nm}, h_{nm} are the coefficients of the spherical harmonic analysis determined from the original data. If the expansion coefficients g_{nm} and h_{nm} are known, we can reconstruct the synoptic map of the magnetic field and analyze its distribution. The method is described in more detail in papers by Hoeksema and Scherrer, 1986; Hoeksema, 1991; Kharshiladze and Ivanov, 1994; and Obridko and Shelting, 2000a.

It should be noted that:

(1) The Mt. Wilson data from August 1965 through Dececember 1978 digitized by Stenflo and the Stanford data after 1976 were obtained in different formats. In order to reduce them to a single format, we, first, calculated the expansion coefficients g_{nm} and h_{nm} for each half-rotation in every format independently. Then, for the overlapping interval (CR 1642–1756, years 1976–1984), we calculated a matrix for converting the coefficients from one format to another in linear approximation. Thus, we obtained coefficients, which allowed all magnetic field vector components to be calculated over the entire time interval under consideration.

(2) Of course, the potential approximation is not very strictly observed at the photospheric level. However, we use the observed line-of-sight field as a lower boundary condition to estimate the coronal field under a potential approximation. We do not assume the large-scale field to be predominantly radial in the photosphere, but calculating the expansion coefficients by a minimization method forces a correlation between B_r and B_θ, which is stronger the larger the field scale. Besides, we used a limited number of the expansion terms ($N = 9$) in our calculations. To test the effect of these limitations, we compared the calculated and observed values of the line-of-sight field component (Obridko, Kharshiladze, and Shelting, 1994). It turned out that the local magnetic fields (the fields of relatively small scale and high intensity) were underrated noticeably, while the large-scale fields of relatively low intensity did not virtually differ from the observed values. Besides, as shown by Harvey and White (1996), the contribution of high-intensity magnetic
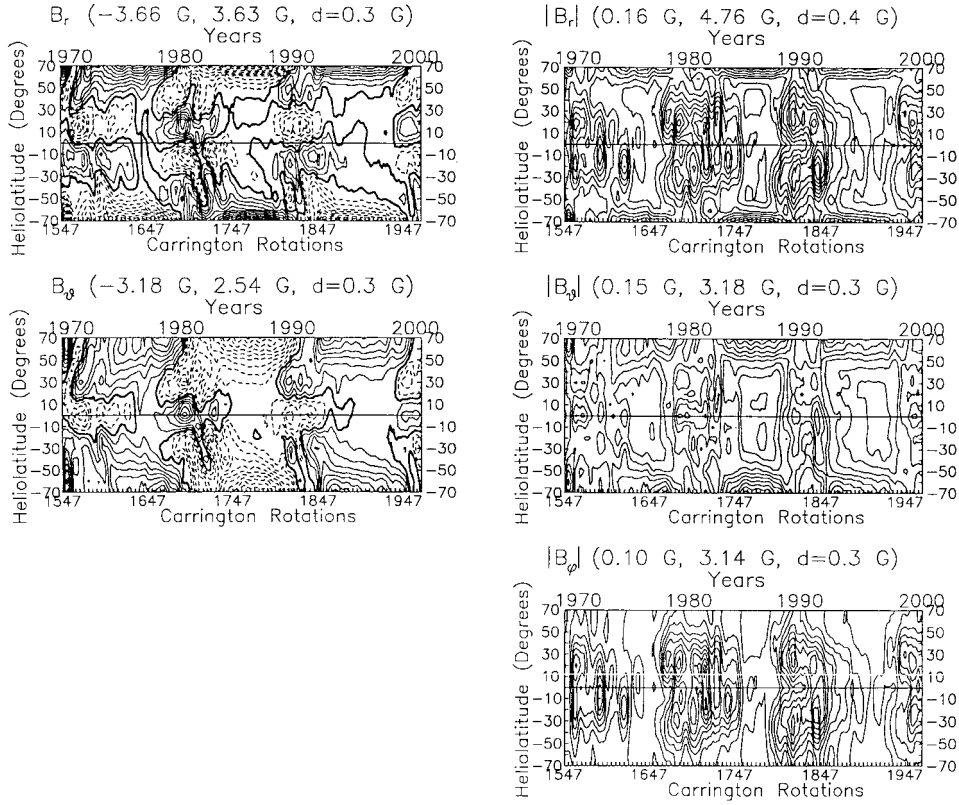
Figure 1. Time−latitude diagrams for B_r, B_θ, $|B_r|$, $|B_\theta|$, and $|B_\varphi|$ smoothed over 8 CR. The figures in brackets above the panels denote (in the order of sequence) the minimum and maximum values of the corresponding parameter and the step between the contours in the panel.

fields of sunspots to the total magnetic flux of the Sun is relatively small, not exceeding ∼10% of the total flux even in the epochs of solar maximum. Thus, we arrived at the conclusion that the calculations described above were perfectly suitable for the statistical analysis of cyclic variations of large-scale magnetic fields under consideration.

After having determined the daily radial B_r, meridional B_θ, and azimuthal B_φ components of the solar magnetic field by formulas (1)–(3), we calculated the mean magnetic field components ($\langle B_r \rangle$, $\langle B_\theta \rangle$, and $\langle B_\varphi \rangle$) and their respective absolute values ($\langle |B_r| \rangle$, $\langle |B_\theta| \rangle$ and $\langle |B_\varphi| \rangle$) by averaging the daily values over one CR. It is clear that, as a result of averaging, the daily values of B_φ over one CR, the mean B_φ component must be zero at each of the 15 heliolatitudes. Besides, the data in the φ direction are always obtained at different times of the field evolution, and this is a further source of noise in that component. Therefore, the B_φ diagram manifests only the distribution of B_φ random errors and will not be considered further.

We used B_r, B_θ, $|B_r|$, $|B_\theta|$, and $|B_\varphi|$ to plot the time−latitude diagrams similar to those used by Hoeksema (1991), Makarov and Sivaraman, (1989), Stenflo (1992), and Benevolenskaya (1998a, b) for the magnetic field longitudinal and radial components. The time−latitude diagram was plotted for each parameter to characterize its cyclic evolution at 15 selected heliolatitudes within the latitude interval under consideration. Similar diagrams were plotted for the same mean parameters smoothed over 4, 6, 8, 14, and 40 CR. As shown by comparison, the results of smoothing over 4, 6, 8, and 14 CR do not differ qualitatively. Therefore, we shall henceforth consider only the values smoothed over 8 and 40 rotations. We also consider the values of the magnetic field components, called further 'quasi-biennial', which were obtained in the following way. First, we obtained two data series by subtracting the values smoothed over 8 and 40 CR from the corresponding unsmoothed field components. After that, the resulting series were subtracted from one another.

These three types of time−latitude diagrams (for values smoothed over 8, 40 CR and 'quasi-biennial' values) allow us to study independently the processes in the magnetic field with characteristic times greater than ~ 0.6 years, greater than ~ 3 years, and in a range of ~ 0.6 to 3 years. The unsmoothed values averaged over one rotation have a high noise component and are not considered in our study.

To study the zonal structure and relationship of LSSMF variations at different latitudes in more detail, we calculated cross-correlation functions (CCF) for each of the 5 parameters (B_r, B_θ, $|B_r|$, $|B_\theta|$, and $|B_\varphi|$) under consideration at the equator and at the other 14 heliolatitudes for the entire time interval of 1969−1996 with a shift up to ± 100 CR. The direction of the correlation lag was determined by correlating each magnetic field parameter at higher heliolatitudes with the same parameter at the equator. The obtained CCF were used to plot correlograms in the 'shift-heliolatitude' reference frame.

3. Study of the Zonal Structure, Meridional Drift, and Cyclic Evolution of LSSMF

Figure 1 illustrates the time−latitude diagrams of B_r, B_θ, $|B_r|$, $|B_\theta|$, and $|B_\varphi|$ averaged over one CR and smoothed over 8 CR at 15 heliolatitudes evenly spaced by 10° in the interval of $\pm 70°$ in the northern and southern hemispheres. In this figure, we can clearly see all basic peculiarities of the LSSMF behavior: the zonal structure, poleward meridional drift, and cyclic evolution. Unlike the time−latitude diagrams plotted for the magnetic field longitudinal or radial component alone, the B_r and B_θ diagrams show the spatial zonal structure in the latitudinal distribution of large-scale magnetic fields more distinctly. In fact, one can readily see that the zones of maximum values of B_r at the B_r diagram correspond to the zones of minimum values of B_θ at the B_θ diagram and *vice versa*. If we imagine a meridional magnetic field line in the form of an arc connecting two neighbouring
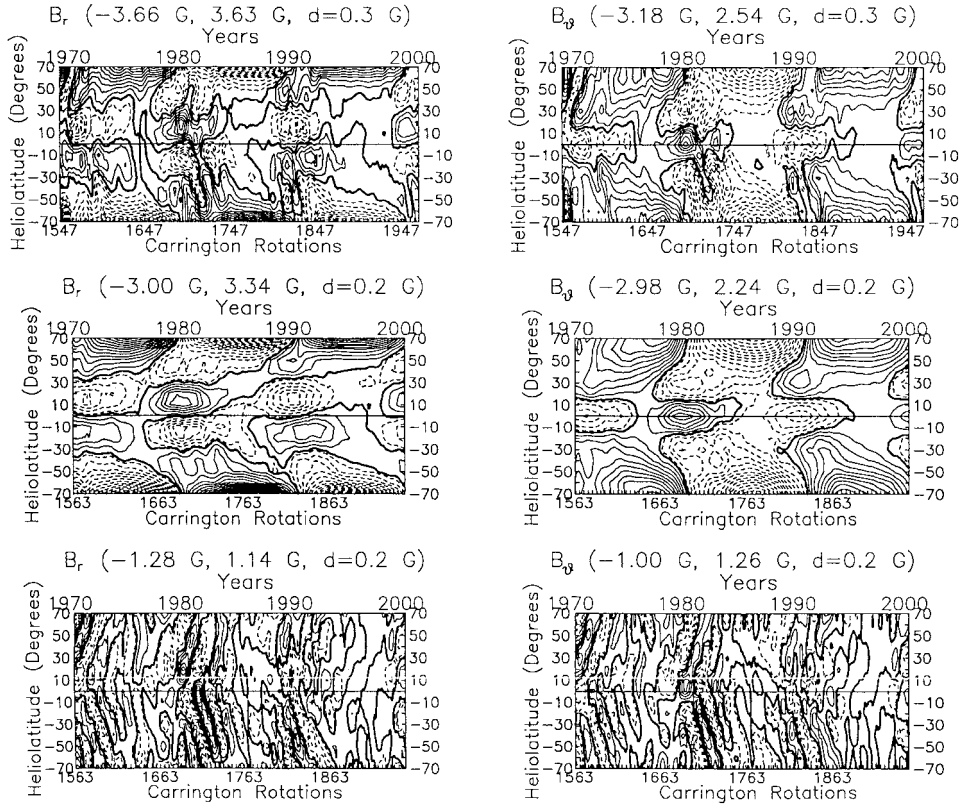
Figure 2. From the top down: time–latitude diagrams for B_r and B_θ smoothed over 8 CR, over 40 CR, and 'quasi-biennial' B_r and B_θ confined to the interval of variation periods from 8 to 40 CR. The figures in brackets above the panels denote (in the order of sequence) the minimum and maximum values of the corresponding parameter and the step between the contours in the panel.

heliolatitudes, then the feet of the arc will correspond to the maximum B_r and, simultaneously, the minimum B_θ; and the apex point, to the minimum B_r and maximum B_θ. This accounts for the shift of the heliolatitudinal zones of alternating polarity in B_θ diagrams with respect to the corresponding zones in B_r diagrams. Besides, independent analysis of B_θ, $|B_\theta|$, B_φ, and $|B_\varphi|$ allows us to study the cyclic behaviour of the poloidal (B_θ, $|B_\theta|$) and toroidal (B_φ, $|B_\varphi|$) field components separately. As noted above, averaging of the daily values of B_φ over one CR makes the mean B_φ component go to zero. However, we can also analyze cyclic variations of $|B_\varphi|$ proportional to the root square energy of the toroidal field component.

The fields in the zones differ both in their intensity and sign. The peak values of B_r are observed at the maxima of the 11-year cycle at the latitudes of about $\pm(15-20°)$ and $\pm 40°$; B_θ maxima take place at the same time, but at the latitudes of about $0°$ and $\pm 30°$. Each component changes its sign when passing from one zone to another. So, we can see four different zones of large-scale magnetic fields

in the equatorial and mid-latitude regions $(< |\pm 50°|)$. With the two polar regions $(> |\pm 50°|)$ taken into account, we observe the total of 6 magnetic field zones of alternating polarity. The zonal structure is most pronounced at the maxima of the 11-year cycle and is much weaker at the minima, when it practically vanishes in B_θ. At the same time, we can only see four zones of maximum magnetic field intensity in the $|B_r|$ and $|B_\theta|$ time−latitude diagrams: one in each of the two mid-latitude (northern and southern) and two polar regions.

The diagrams for B_r and B_θ show pronounced 22-year cyclic variations of LSSMF in both mid- and high-latitude regions, and the diagrams for $|B_r|$, $|B_\theta|$, and $|B_\varphi|$ display an 11-year cycle. However, in the equatorial and mid-latitude regions $(< |\pm 50°|)$, B_r, B_θ, $|B_r|$, and $|B_\theta|$ reach their peak values in the maximum epochs of the 11-year cycles and in the high-latitude zones $(> |\pm 50°|)$, in the minimum epochs. I.e., they are shifted in phase by about 5 years with respect to the similar maximum values in the mid-latitude zones. The values $|B_r|$, $|B_\theta|$ and $|B_\varphi|$ also reveal an asymmetry in heliolatitudinal distribution of large-scale magnetic fields, which is most pronounced in the maximum epochs of the 11-year cycle. The asymmetry changes its direction and value from one activity cycle to another.

As seen from Figure 1, B_r and B_θ zones display two types of the behavior: a slow drift of the zone centers from the equator to the poles for a time of $\sim$16−18 years and a much faster motion in the same direction, which takes $\sim$30−40 solar rotations (i.e., about 2−3 years). In the time−latitude diagrams for B_r they look as 'tongues' of magnetic fields of one sign extending to high latitudes. If we count the drift time from the appearance of a certain polarity zone at the equator till its disappearance (change of polarity) at the poles, it will make up about 22 years.

In order to analyze each type of the drift (slow and fast) separately, we plotted (Figure 2 from the top down) the time−latitude diagrams for B_r and B_θ smoothed over 8 CR, over 40 CR, and B_r and B_θ in the interval of periods from 8 to 40 CR ('quasi-biennial' variations). In this figure, we can distinctly see two types of meridional poleward drift of zonal structures: a 16−18-year drift for B_r and B_θ smoothed over 40 CR (middle panels) and a 2−3 year drift for B_r and B_θ confined to the variation periods from 8 to 40 CR (lower panels). In the first case, the lifetime of a polarity zone at a certain heliolatitude is, on the average, $\sim$11 years; and in the second, $\sim$15−20 rotations ($\sim$1.5 years). The two types of the meridional drift are shown superimposed in the upper panel.

Figure 3 shows the time−latitude diagrams for $|B_r|$, $|B_\theta|$ and $|B_\varphi|$ analogous to the diagrams for B_r and B_θ in Figure 2. As seen from Figure 3, the drift for $|B_r|$, $|B_\theta|$ and $|B_\varphi|$ is virtually absent or even has the equatorward direction as in the case of $|B_r|$ and $|B_\varphi|$ smoothed over 8 or 40 CR. One can see a pronounced difference between the mid- and high-latitude regions. The maximum values of $|B_r|$ and $|B_\theta|$ proportional to the square root of energy of the corresponding field components at mid latitudes are shifted by 5−5.5 years with respect to the maximum values of these parameters at high latitudes. This implies the pumping of energy from the mid-latitude to high-latitude region and back for a time equal to about half of the
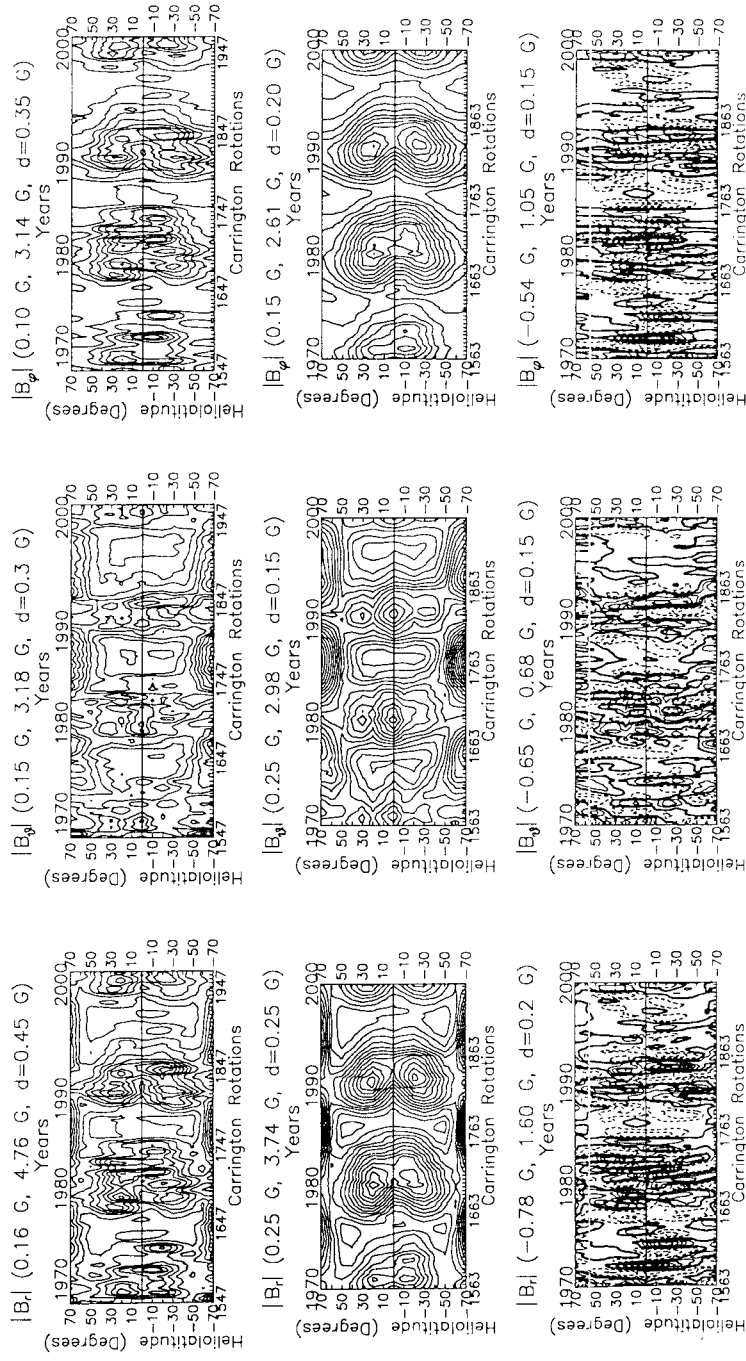
Figure 3. From the top down: time–latitude diagrams for $|B_r|$, $|B_\theta|$ and $|B_\varphi|$ smoothed over 8 CR, over 40 CR, and 'quasi-biennial' B_r and B_θ confined to the interval of variation periods from 8 to 40 CR. The figures in brackets above the panels denote (in the order of sequence) the minimum and maximum values of the corresponding parameter and the step between the contours in the panel.
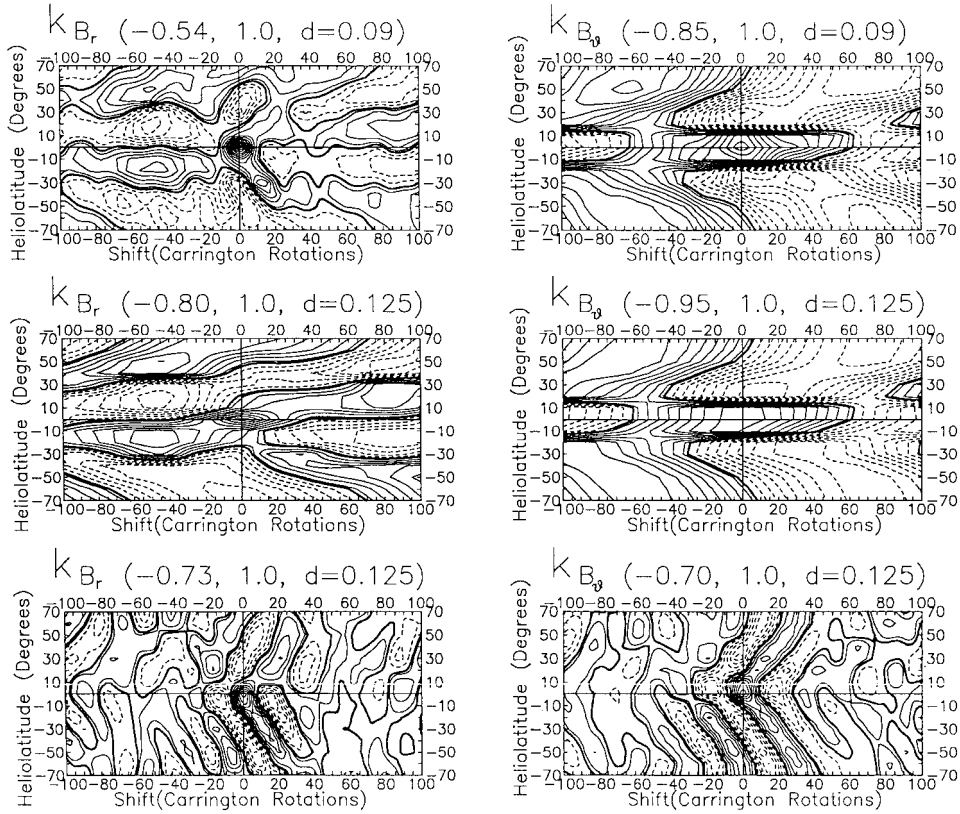
Figure 4. Cross-correlation of B_r and B_θ at the equator with their respective values at the other 14 selected heliolatitudes spaced by $10°$ in the northern and southern hemispheres for the time interval of 1969–2000. *From the top down*: B_r and B_θ smoothed over 8 CR, over 40 CR, and 'quasi-biennial' B_r and B_θ confined to the interval of variation periods from 8 to 40 CR. The figures in brackets above the panels denote (in the order of sequence) the minimum and maximum correlation coefficients and the step between the contours in the panel.

11-year cycle. One can also see quasi-biennial oscillations of $|B_r|$ and $|B_\varphi|$ in the mid-latitude zones.

Additional information on the relationship between LSSMF variations at the equator and at higher latitudes can be obtained from the correlograms plotted for each of the 5 magnetic field components. Figure 4 illustrates the correlograms obtained by correlating B_r and B_θ at the equator with their respective values at each of the 14 selected heliolatitudes for the time interval of 1969–2000. The direction of the correlation lag was determined by correlating a magnetic field parameter at higher heliolatitudes with same parameter at the equator. The correlograms are plotted (from the top down) for B_r and B_θ smoothed over 8 CR, over 40 CR, and B_r and B_θ in the interval of periods from 8 to 40 CR ('quasi-biennial' variations). The figure reveals a pronounced zonal structure of large-scale magnetic fields and their
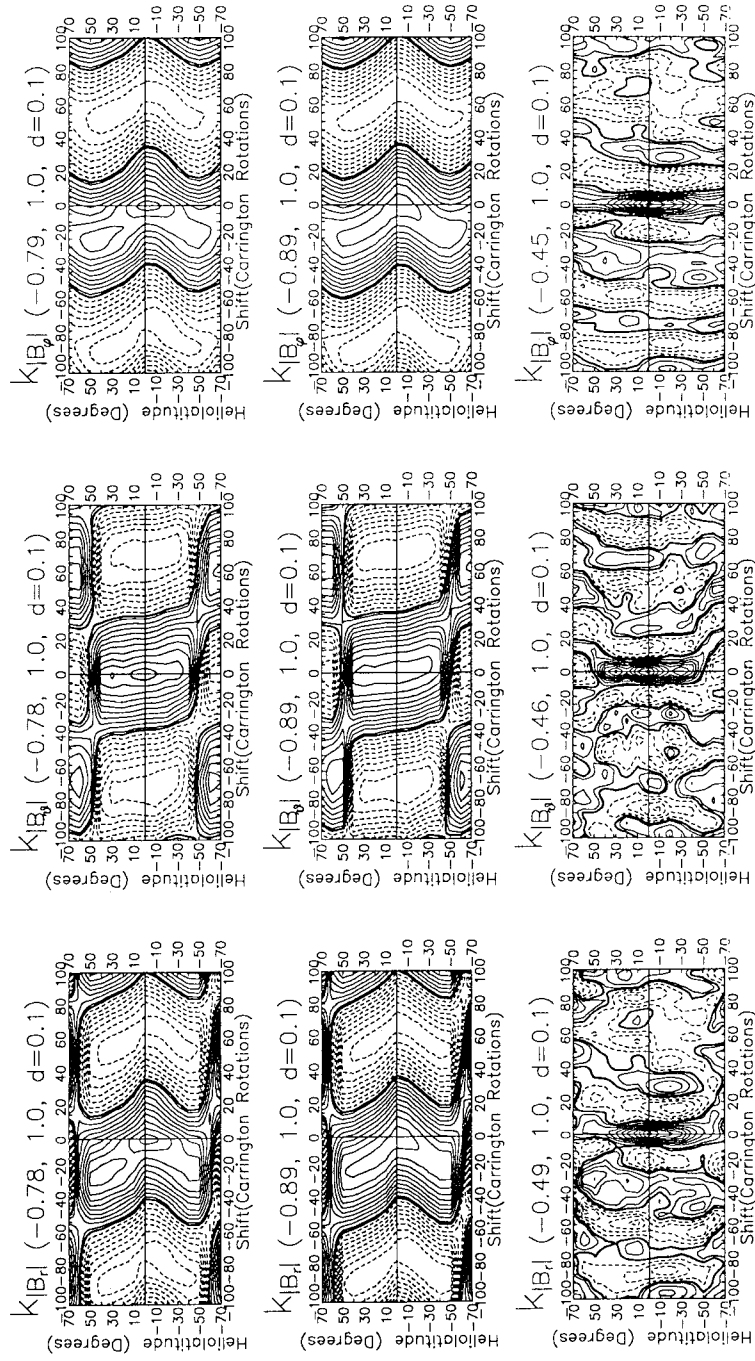
Figure 5. Cross-correlation of $|B_r|$, $|B_\theta|$, and $|B_\varphi|$ at the equator with their respective values at the other 14 selected heliolatitudes spaced by 10° in the northern and southern hemispheres for the time interval of 1969–2000. *From the top down:* $|B_r|$, $|B_\theta|$, and $|B_\varphi|$ smoothed over 8 CR, over 40 CR, and 'quasi-biennial' B_r, $|B_\theta|$, and $|B_\varphi|$ confined to the interval of variation periods from 8 to 40 CR. The figures in brackets above the panels denote (in the order of sequence) the minimum and maximum correlation coefficients and the step between the contours in the panel
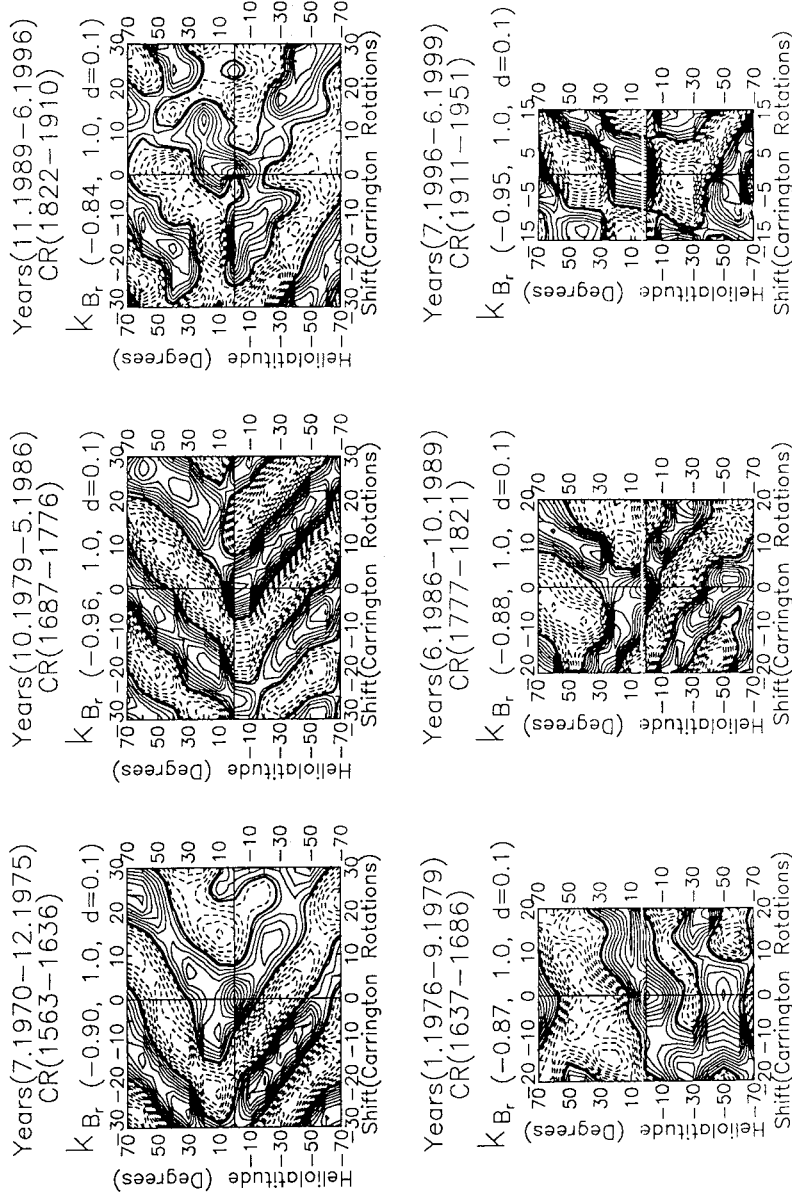
Figure 6a. Cross-correlation of 'quasi-biennial' values of B_r at the equator and at the other 14 heliolatitudes spaced by 10° in the northern and southern hemispheres in the growth and decay phases of cycles 20–23. The figures in brackets above the panels denote (in the order of sequence) the minimum and maximum correlation coefficients and the step between the contours in the panel.

Figure 6a. Cross-correlation of 'quasi-biennial' values of B_θ at the equator and at the other 14 heliolatitudes spaced by 10° in the northern and southern hemispheres in the growth and decay phases of cycles 20–23. The figures in brackets above the panels denote (in the order of sequence) the minimum and maximum correlation coefficients and the step between the contours in the panel.
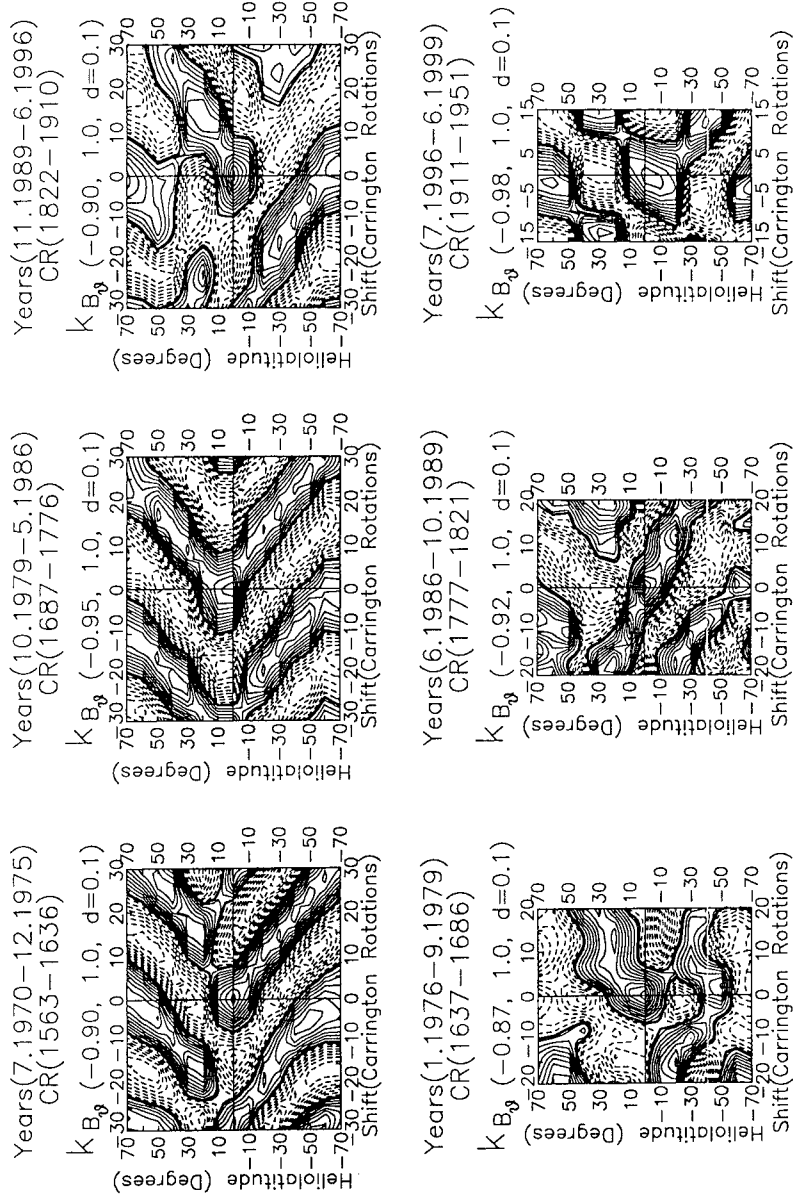
poleward drift. In fact, one can see two types of the drift from the equator to the poles with characteristic times of the order of 16−18 years and about 2−3 years. It should be noted that the correlogram for B_r smoothed over 8 CR displays both types of the drift, while the similar correlogram for B_θ displays only the drift with a characteristic time of 16−18 years. Thus, the dipole (poloidal) part of the magnetic field, which is responsible for the 11-year variation, is predominant in B_θ, whereas in B_r, both parts of the magnetic field (poloidal and toroidal) exist. In fact, it is the toroidal field that accounts for the higher-order fields, which are responsible for the 2−3-year variation and display a fast drift with characteristic times of about 2−3 years. We should remember that, during most of the 11-year cycle, quasi-biennial oscillations are observed in the mid-latitude zone alone confined by the polar filaments. It is only when the latter reach the poles during the field reversal at the maximum of the cycle that QBO penetrate the polar zones (Benevolenskaya and Makarov, 1990, 1992; Benevolenskaya, 1996; Ivanov, Obridko, and Ananyev, 2001). Cyclic variations in the latitudinal extension of the mid-latitude zone confined by the polar filaments, i.e., the shift of its boundaries to the poles in the growth phase and to the equator in the decay phase, are probably due to the enhancement or weakening of toroidal fields in the process of their generation during the 11-year cycle.

The correlograms for both components (B_r and B_θ) in the interval of periods from 8 to 40 CR reveal a clear poleward drift with a characteristic time of about 2−3 years ($\sim$30−40 rotations) and with the zones of opposite polarities alternating in $\sim$15−20 rotations. I.e., 'quasi-biennial' magnetic-field oscillations (with a period of $\sim$30−40 rotations equal to the double polarity-reversal period) drift from the equator to high latitudes for a time of about 2−3 years ($\sim$30−40 rotations). It is interesting to note that both types of the drift have a distinct quasi-periodic nature. The CCF maxima are repeated each 70−80 rotations (5−6 years) for the drift with a characteristic time of 16−18 years and each 15−20 rotations ($\sim$1−1.5 years) for the drift with a characteristic time of 2−3 years.

Figure 5 illustrates the correlograms for $|B_r|$, $|B_\theta|$ and $|B_\varphi|$ analogous to those shown in Figure 4 for B_r and B_θ. Unlike the correlograms in Figure 4, the correlograms for $|B_r|$, $|B_\theta|$ and $|B_\varphi|$ display an essential difference between the mid-latitude and polar zones. As seen in Figure 5, the variations of $|B_r|$ and $|B_\theta|$ display a positive correlation virtually all over the mid-latitude zone with a shift of about $\pm$20 rotations. On the other hand, the correlation between the equatorial and high-latitude variations of $|B_r|$ or $|B_\theta|$ is negative, a positive correlation being only observed when respective variations occur with a shift of about $\pm$(60−70) CR (i.e., $\sim$5−5.5 years). This means that negative correlation between the $|B_r|$ (or $|B_\theta|$) values in the mid and high-latitude zones at every given moment turns to positive as variations at the poles shift by $\pm$(60−70 CR) (i.e., $\sim$5−5.5 years) with respect to variations at the equator. This points to a close connection of global magnetic field variations in the mid- and high-latitude zones and may account for the apparently causal relationship between the occurrence rate and intensity of the

polar faculae and mid-latitude sunspots observed about 5 years later (Makarov and Makarova, 1996). This relationship implies that the global magnetic field of polar region is primary with respect to the toroidal fields of mid-latitudinal zone. This conclusion follows also from Makarov *et al.* (2001). The correlation between the equatorial and high-latitude variations in $|B_\varphi|$ is also different and indicates opposite direction of the $|B_\varphi|$ drift in the mid-latitude and polar zones. But this result needs examination, because $|B_\varphi|$ is very small in polar zones.

It is interesting to note that the poleward drift is only pronounced in B_r and B_θ, but is virtually absent in $|B_\theta|$ or even has an opposite direction in $|B_r|$ and $|B_\varphi|$ in mid-latitude zones. A fast drift towards the equator (by ~ 50–$60°$ for ~ 20–30 rotations) is observed in the mid-latitude zone for $|B_r|$ and $|B_\varphi|$ smoothed over 8 and 40 CR. For 'quasi-biennial' $|B_r|$, $|B_\theta|$ and $|B_\varphi|$ confined to the interval of variation periods from 8 to 40 CR, the drift is absent. This is, probably, indicative of the fact that the sources of 'quasi-biennial' oscillations of the magnetic field remain invariable, while the fast poleward drift of B_r and B_θ may be due to redistribution of large-scale magnetic fields on the solar surface caused by some external forces (presumably, by sub-surface plasma flows in the convection zone or by the field-line shear as the magnetic fields emerge to the solar surface from the toroidal field generation region at the bottom of the convection zone).

The 2–3-year oscillations and the poleward drift of the magnetic fields are seen in even more detail from the correlograms for quasi-biennial B_r (Figure 6a) and B_θ (Figure 6b) plotted separately for the growth and the decay epochs of cycles 20–23. The character of the drift changes from cycle to cycle, as well as in different phases of one cycle. The drift (or magnetic field reconstruction) during a cycle is pulse-like with a characteristic period of ~ 10–20 CR (~ 1–1.5 year) and displays an asymmetry between the northern and southern hemispheres both in its velocity and character.

4. Conclusions

The main results of our study can be summarized as follows:

(1) Besides the 11-year cyclic variations in the mid- and high-latitude (polar) zones observed in the time–latitude diagrams for $|B_r|$ and $|B_\theta|$, the large-scale solar magnetic field also displays a phase delay of about $\pm(65$–$70)$ CR (~ 5–5.5 years) between the field variations in the mid- and high-latitude regions. This may account for the causal relationship between the occurrence rate and intensity of the polar faculae and mid-latitude sunspots observed ~ 5 year later (Makarov and Makarova, 1996).

(2) Along with a relatively simple zonal structure of the solar magnetic field consisting of two mid-latitude ($< |\pm 50°|$) and two polar ($> |\pm 50°|$) zones, which is seen in the time–latitude diagrams and correlograms for $|B_r|$ and $|B_\theta|$, a more complicated zonal structure is observed in the diagrams for B_r and B_θ. It

comprises four zones of magnetic field of alternating polarity in the mid-latitude and equatorial regions and two zones in polar regions. With two polar zones taken into account, we observe a total of six magnetic field zones of alternating polarity. This zonal structure drifts away from the equator at a velocity of ~ 2–3 m s^{-1}, reaching the poles in about 16–18 years.

(3) Besides the evolutionary changes over 22 years and the zonal structure of LSSMF, the time–latitude diagrams and correlograms for B_r and B_θ reveal variations of magnetic fields with a quasi-period of ~ 20–30 CR (i.e., ~ 2–3 years) and a poleward drift of the same duration. Furthermore, we can clearly distinguish between two types of the poleward meridional drift: the 16–18-year drift and the 2–3 year drift. Both the 16–18-year and the 2–3-year drifts have a pronounced quasi-periodic nature. The CCF maxima of B_r and B_θ variations are repeated each 70–80 rotations (5–6 years) for the drift with a characteristic time of 16–18 years and each 15–20 rotations (~ 1–1.5 years) for the drift with a characteristic time of 2–3 years. In the diagrams for $|B_r|$ and $|B_\theta|$, the 'quasi-biennial' variations and both types of the drift are virtually absent or even have an opposite (equatorward) direction. This implies that the drift observed in B_r and B_θ can be due to re-distribution of large-scale magnetic fields on the solar surface caused by some external forces (presumably, by sub-surface plasma flows in the convection zone).

(4) Most figures display a noticeable asymmetry in the distribution of large-scale solar magnetic fields relative to the equator. One can also see an asymmetry in the velocity and character of the ~ 2–3 year drift between the northern and southern hemispheres. The asymmetry changes from cycle to cycle, as well as with the phase of the activity cycle.

The results obtained in this study suggest the existence of two different processes of organization and redistribution of magnetic fields in the Sun. One of them (call it conventionally the 'energy process') is illustrated in the time–latitude diagrams and correlograms for $|B_r|$, $|B_\theta|$ and $|B_\varphi|$. It covers a broad range of heliolatitudes from $+70°$ to $-70°$ and does not comprise drift. This implies that the process under consideration occurs in a region where the differential rotation is absent, i.e., at the bottom of the convection zone or immediately under it. The process manifests itself in ~ 10–11-year oscillations of intensity of the global magnetic field between the mid- and high-latitude regions and can be directly related to the mechanism of generation of solar magnetic fields. LSSMF variations in the mid-latitude zone display a phase delay of about 65–70 CR (~ 5–5.5 years) with respect to the variations in the high-latitude zone.

Another process (call it 'structuring') is illustrated in the time–latitude diagrams and correlograms for B_r and B_θ and manifests itself as fast-drifting zonal structures. This process may be related to re-distribution of large-scale magnetic fields as they emerge from the field generation region to the solar surface and is due to some external forces (presumably, by sub-surface plasma flows in the convection zone or by the field-line shear as the magnetic fields emerge to the solar surface from the toroidal field generation region at the bottom of the convection

zone). We believe that the process of redistribution of large-scale magnetic fields is precisely what accounts for quasi-biennial oscillations of LSSMF and the poleward drift of the same duration.

According to helioseismological studies (e.g., see Giles *et al.*, 1997; Giles, Duvall, and Scherrer, 1998; Giles and Duvall, 1998; Giles, 1999), the meridional circulation is a global phenomenon not confined to the solar surface alone. The helioseismic measurements are consistent with the presence of a single circulation cell in each hemisphere with a poleward flow of $\sim$20 m s^{-1} at the surface and an equatorward velocity of about 3 m s^{-1} at the base of the convection zone. The turning point for the circulation is at $r = 0.80 \, R_0$, where R_0 is the radius of the Sun. Simultaneously, one can see in the Sun a pattern consisting of bands of faster-than-average and slower-than-average rotation ('torsional oscillation'), which moves towards the equator (Howard and LaBonte, 1980; Snodgrass and Howard, 1985a, b; Ulrich *et al.*, 1988). This pattern is repeated on a time scale of 10–20 years and its behavior is strikingly similar to the well-known butterfly diagram of solar magnetic activity. Makarov and Tlatov (1997) and Callebaut *et al.* (1999) show that the bands of slower-than-average rotation appear after the reversal of the polar magnetic field and migrate to the equator on the time–latitude diagram during 7–15 years along the butterfly diagrams of polar faculae and sunspots. The bands of faster-than-average rotation appear 5–6 years later. The latitudinal drift of the bands is connected with the solar activity. The surplus poloidal component V_θ varies from 2 to 6 m s^{-1}. From 1975 to 1995, the value of V_θ did not exceed 4 m s^{-1}. The torsional oscillations are clearly seen at the solar surface, but helioseismic observations reveal no evidence of the torsional oscillation pattern below 0.92–0.95 R_0 (Giles *et al.*, 1997; Giles, 1999; Schou, 1999; Howe, Komm, and Hill, 1999; Howe *et al.*, 2000; Antia and Basu, 2000). Thus, we observe two opposite (poleward and equatorward) meridional flows. The poleward flow consists of two modes: a slow mode with a speed of $\sim$3 m s^{-1} and the drift time from the equator to the pole or vice versa of about 16–18 years and a fast mode in the mid-latitude ($< | \pm 50°|$) region with a speed of $\sim$20 m s^{-1} and the drift time from the mid to high latitudes of $\sim$2–3 years. The opposite equatorward flow contains only one, slow mode (see also Giles *et al.*, 1997; Giles, Duvall, and Scherrer, 1998; Giles and Duvall, 1998; Giles, 1999). We suggest that the slow poleward drift of the magnetic field zonal structure with a speed of $\sim$2–3 m s^{-1} and characteristic time of $\sim$16–18 years revealed in our work, the equatorward flow with the same velocity at the base of the convection zone calculated by Giles, and the pattern of bands of faster-than-average and slower-than-average rotation ('torsional oscillation'), which propagates towards the equator approximately for the same time, are manifestations of the global magnetic field. In helioseismological studies, this flow is not observed in pure form unless at the poles or near the equator. In the mid-latitude zone, the poleward meridional flow at $\sim$20 m s^{-1} observed by Giles (1999) is apparently the sum of the slow and fast drift modes with the prevailing contribution of the fast drift. The comparison of $|B_r|$, $|B_\theta|$, and $|B_\varphi|$ time–latitude diagrams

in Figure 1 shows that the main contribution to the magnetic flux at mid-latitudes is made by the toroidal field component, which manifests itself in $|B_\varphi|$ and, partly, in $|B_r|$. Therefore, the fast drift in the mid-latitude zone may be a manifestation of the toroidal field component. Simultaneously with the $\sim 2-3$-year poleward drift, one can see quasi-biennial variations of the magnetic field in the form of a zonal structure moving quickly to the poles. However, their relation to the $\sim 2-3$-year drift is not clear yet. Quasi-biennial variations can probably be accounted for in terms of one of the two dynamo mechanisms proposed by Benevolenskaya (1998) in her model of the double magnetic cycle of the Sun. Interpretation of both the slow and fast drift modes should obviously be based on a model explaining the balance of the angular momentum in the convection shell of the Sun in terms of interplay of the meridional and convective motions.

5. Acknowledgements

References

Ambrož, P.: 1992, in S. Fisher and M. Vandas (eds.), *Proceedings of the First SOLTIP Symposium*, Vol. **21**, pp. 38–53.

Ananyev, I. V. and Obridko, V. N.: 1999, *Astron. Rep.* **43**, 831.

Antia, H. M. and Basu, S.: 2000, *Astrophys. J.* **541**, 442.

Antonucci, E., Hoeksema, J. T., and Scherrer, P. H.: 1990, *Astrophys. J.*, **360**, 296.

Benevolenskaya, E. E.: 1996, *Solar Phys.* **167**, 47.

Benevolenskaya, E. E.: 1998a, *Astrophys. J.* **509**, L49.

Benevolenskaya, E. E.: 1998b, *Solar Phys.* **181**, 479.

Benevolenskaya, E. E. and Makarov, V. I.: 1990, *Soln. Dann.*, No. 5, 75–79.

Benevolenskaya, E. E. and Makarov, V. I.:1992, *Pisma Astron. Zh.* **3**, 266–270.

Benevolenskaya, E. E., Hoeksema, J. T., Kosovichev, A. G. and Scherrer, P. H.: 1999, *Astrophys. J.* **517**, L163.

Callebaut, D. K., Gelfreikh, G. B., Makarov, V. I., Shibasaki, K. and Tlatov, A. G.: 1999, in A. Wilson (ed.), *Magnetic Fields and Solar Processes, Proceedings of Ninth European Meeting on Solar Physics*, Florence, Italy, 12–18 September 1999, ESA SP Series, SP-448.

Duvall, T. L.: 1979, *Solar Phys.* **63**, 3.

Erofeev, D. V.: 1997, *Solar Phys.* **175**, 45.

Erofeev, D. V.: 1999, *Solar Phys.* **187**, 185.

Giles, P. M.: 1999, A Dissertation for the Degree of Dr. Ph., Stanford University, Stanford.

Giles, P. M. and Duvall, T. L., Jr.: 1998, in F.-L. Deubner *et al.* (eds.), 'New Ways to See Inside the Sun and Stars', *Proceedings IAU Symp.* **185**, 149.

Giles, P. M., Duvall Jr., T. L. and Scherrer, P. H.: 1998, in S. G. Korzennik and A. Wilson (eds.), *Structure and Dynamics of the Sun and Sun-Like Stars, Proceedings of SOHO6/GONG98 Workshop*, Noordwijk, ESA Publication Division, p. 175.

Giles, P. M., Duvall Jr., T. L., Scherrer, P. H. and Bogart, R. S.: 1997, *Nature,* **390**, 52.

Harvey, K. L. and White, O. R.: 1996, *Solar Magnetic Fields: the Key to Understanding Solar Irradiance Variations*, SPRC Technical Report 96–01.

Hoeksema, J. T.: 1991, *Solar Magnetic Field 1985 through 1990*, WCDA, Boulder, U.S.A.

Hoeksema, J. T. and Scherrer P. H.: 1986, *Solar Magnetic Field 1976 through 1985*, WCDA, Boulder, U.S.A.

Hoeksema, J. T. and Scherrer, P. H.: 1987, *Astrophys. J.* **318**, 428.

Howard, R. and LaBonte, B. J.: 1980, *Astrophys. J.* **239**, L33.

Howard, R. F., Harvey, J. W. and Forgach, S.: 1990, *Solar Phys.* **130**, 295.

Howe, R., Komm, R. and Hill, F.: 1999, *Astrophys. J.* **524**, 1084.

Howe, R., Christensen-Dalsgaard, J., Hill, F., Komm, R. *et al.*: 2000, *Astrophys. J.* **533**, L163.

Ivanov, E. V.: 1986, *Soln. Dann.* **7**, 61.

Ivanov, E. V: 1994, in D. D. Baker, V. O. Papitashvili, and M. J. Teague (eds.), *Solar-Terrestrial Energy Program, The Initial Results from STEP Facilities and Theory Campaigns, Proceedings of the 1992 STEP Symposium/5th COSPAR Colloquium*, held in Laurel, Maryland, U.S.A., 24–28 August 1992, Pergamon, *COSPAR Colloquia Series* **5**, 133.

Ivanov, E. V.: 1995, *Bull. Russ. Acad. Sci. Phys.* **59**, 1133.

Ivanov, E. V., Obridko, V. N. and Ananyev, I. V.: 2001, *Solar Phys.* **199**, 405.

Kharshiladze, A. F. and Ivanov, K. G.: 1994, *Geomagn. Aeron.* **34**, 22.

Komm, R. W., Howard, R. and Harvey, J. W.: 1993a, *Solar Phys.* **145**, 1.

Komm, R. W., Howard, R. and Harvey, J. W.: 1993b, *Solar Phys.* **147**, 207.

LaBonte, B. J. and Howard, R. F.: 1982, *Solar Phys.* **80**, 361.

Makarov, V. I. and Makarova, V. V.: 1996, *Solar Phys.* **163**, 267.

Makarov, V. I. and Sivaraman, K. R.: 1989, *Solar Phys.* **123**, 367.

Makarov, V. I. and Tlatov, A. G.: 1997, *Astron. Zh.* **74**, 474.

Makarov, V. I., Tlatov. A. G., Callebaut, D. K., Obridko, V. N. and Shelting, B. D.: 2001, *Solar Phys.* **198**, 409.

McIntosh, P. S.: 1972, *Rev. Geophys. Space Phys.* **10**, 837.

McIntosh, P. S.: 1992, in M. Summerfeld (ed.), *Solar Activity Observations and Predictions, Progress in Astronautics and Aeronautics*, Vol. 30, Academic Press, New York, p. 65.

Obridko, V. N., Kharshiladze, A. F. and Shelting, B. D.: 1994, *Solar Magnetic Fields and Helioseismology*, Nauka, Moscow, p. 71.

Obridko, V. N. and Shelting, B. D.: 1997, in V. I. Makarov and V. N. Obridko (eds.), *Present-Day Problems of Solar Cycles*, GAO, St. Petersburg, p. 193.

Obridko, V. N. and Shelting, B.D.: 1998, in V. I. Makarov and V. N. Obridko (eds.), *New Cycle of Solar Activity: Observations and Theory*, GAO, St. Petersburg, p. 137.

Obridko, V. N. and Shelting, B. D.: 1999, *Solar Phys.* **184**, 187.

Obridko, V. N. and Shelting, B. D.: 2000a, *Astron. Zh.* **77**, 124.

Obridko, V. N. and Shelting, B. D.: 2000b, *Astron. Zh.* **77**, 303..

Snodgrass, H. B.: 1983, *Astrophys. J.* **270**, 288.

Snodgrass, H. B.: 1984, *Solar Phys.* **94**, 13.

Snodgrass, H. B. and Howard, R. F.: 1985a, *Solar Phys.* **95**, 221.

Snodgrass, H. B. and Howard, R. F.: 1985b, *Science* **228**, 945.

Snodgrass, H. B. and Ulrich, R. K.: 1990, *Astrophys. J.* **351**, 309.

Schou, J.: 1999, *Astrophys. J.* **523**, L181.

Stenflo, J. O.: 1974, *Solar Phys.* **36**, 495.

Stenflo, J. O.: 1989, *Astron. Astrophys.* **210**, 403.

Stenflo, J. O.: 1992, in K. L. Harvey (ed.), *Proceedings of the National Solar Observatory/Sacramento Peak 12th Summer Workshop*, San Francisco, California, 421.

Ulrich, R. K.: 1998, in *SOHO 6/GONG 98 Workshop Abstract*, June 1–4, Boston, Massachusetts, p. 851.

Ulrich, R. K., Boyden, J. E., Webster, L., Snodgrass, H. B., Padilla, S. P., Gilman, P. and Scheiber, T.: 1988, *Solar Phys.* **117**, 291.

Wilcox, J. M. and Howard, R. F.: 1970, *Solar Phys.* **13**, 251.

Wilson, P. R.: 1994, *Solar and Stellar Activity Cycles*, Cambridge University Press, Cambridge.